

Stealthy Patch-Wise Backdoor Attack in 3D Point Cloud via Curvature Awareness

Yu Feng¹ Dingxin Zhang¹ Runkai Zhao¹ Yong Xia² Heng Huang³ Weidong Cai¹

¹ The University of Sydney

² Northwestern Polytechnical University ³ University of Maryland College Park

{yfen0146, dzha2344, rzha9419} @uni.sydney.edu.au

yxia@nwpu.edu.cn heng@umd.edu tom.cai@sydney.edu.au

Abstract

Backdoor attacks pose a severe threat to deep neural networks (DNN) by implanting hidden backdoors that can be activated with predefined triggers to manipulate model behaviors maliciously. Existing 3D point cloud backdoor attacks primarily rely on sample-wise global modifications, resulting in suboptimal stealthiness. To address this limitation, we propose *Stealthy Patch-Wise Backdoor Attack (SPBA)*, which employs the first patch-wise trigger for 3D point clouds and restricts perturbations to local regions, significantly enhancing stealthiness. Specifically, SPBA decomposes point clouds into local patches and evaluates their geometric complexity using a curvature-based patch imperceptibility score, ensuring that the trigger remains less perceptible to the human eye by strategically applying it across multiple geometrically complex patches with lower visual sensitivity. By leveraging the Graph Fourier Transform (GFT), SPBA optimizes a patch-wise spectral trigger that perturbs the spectral features of selected patches, enhancing attack effectiveness while preserving the global geometric structure of the point cloud. Extensive experiments on ModelNet40 and ShapeNetPart demonstrate that SPBA consistently achieves an attack success rate (ASR) exceeding 96.5% across different models while achieving state-of-the-art imperceptibility compared to existing backdoor attack methods.

1. Introduction

Point clouds serve as a highly effective data structure for representing 3D geometric data [10], finding increasing utility in safety-critical applications including autonomous driving [14], healthcare [21, 41], and robotics [47]. With this expanding deployment, the security of point cloud models becomes paramount, particularly concerning their vulnerability to backdoor attacks [13]. In these attacks, ad-

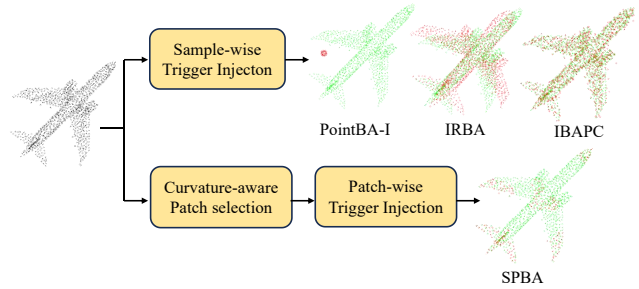


Figure 1. Comparison of sample-wise and patch-wise trigger injection in 3D point cloud backdoor attacks. Green points represent original samples, while red points indicate modifications introduced by injected triggers.

versaries inject a pre-defined trigger into a small portion of training data. This manipulation causes the backdoored model, upon training, to consistently misclassify samples containing the trigger into a target class, while maintaining accurate predictions for benign inputs. A well-designed trigger remains inconspicuous within the data yet potentially activates malicious behavior in the compromised model. Therefore, trigger design is crucial for both the effectiveness and stealth of backdoor attacks [18, 30, 35].

Early explorations into 3D point cloud backdoor attacks utilized direct global geometric modifications as triggers, such as adding spherical point clusters or applying specific rotations [13, 37, 42]. These global modifications produce deformations readily discernible to the human eye and susceptible to standard data preprocessing techniques like Statistical Outlier Removal (SOR) [45] or rotation augmentation [7]. Recent efforts have shifted towards incorporating local context into trigger design to enhance stealthiness. For instance, IRBA [7] utilized a nonlinear and local transformation to generate sample-wise triggers, while IBAPC [5] employed spectral triggers to balance global shape preservation with localized point perturbations. These triggers are

more adaptable, fitting the local geometric structure of samples [7] while preserving the overall global geometry for enhanced stealthiness [5]. However, these methods do not sufficiently focus on local context, limiting their potential for improved concealment. Their triggers either alter the spatial relationship between local and global structures or induce broader deformations, even when aiming for local perturbations.

To this end, we aim to design a novel and highly covert backdoor attack trigger that solely leverages local context information for subtle local modifications. In the 2D image domain, local triggers are typically designed as unified patch-wise triggers [9, 27], which blend seamlessly into diverse image backgrounds. However, the absence of an inherent grid structure in 3D point clouds makes it challenging to design and inject consistent patch-wise deformation triggers without introducing noticeable anomalies or compromising geometric integrity. To address this challenge, we design the patch-wise trigger in the spectral domain rather than the raw spatial domain. By transforming local patches into the spectral domain, we can preserve low-frequency components to maintain the overall local geometric structure while modifying high-frequency components to alter point-level fine-grained details. These modifications are confined within the patch, ensuring precision and subtlety. Furthermore, the patch-wise trigger allows us to selectively perturb specific regions of the point cloud. As noted by [22], human perception varies across different regions of a 3D point cloud, with perturbations in geometrically complex areas being less perceptible. Building on this insight, we selectively filter out smooth patches and apply the patch-wise trigger exclusively to geometrically complex regions, thereby enhancing stealthiness, as illustrated in Figure 1.

In this paper, we propose the Stealthy Patch-Wise Backdoor Attack (SPBA), which introduces the first patch-wise trigger for 3D point cloud backdoor attack. Our approach first decomposes a point cloud sample into local patches, enabling finer control over trigger injection. To select geometrically complex patches, we design a curvature-based Patch Imperceptibility Score (PIS) to quantify patch complexity. The patches with high PIS are selected and then converted into k-nearest neighbors graphs, providing a structured representation of local geometric relationships. We employ the Graph Fourier Transform (GFT) to map point coordinates into the spectral domain, where perturbations can be introduced in a controlled and structured manner. To maintain the geometric integrity of the affected patches, we apply an optimized spectral trigger that selectively modifies the spectral components while preserving the geometric structure of the local patch. Finally, the Inverse Graph Fourier Transform (IGFT) is utilized to reconstruct the poisoned patches, which are then aggregated with the unmodified regions to form the final poisoned point

cloud sample. An alternating optimization process is employed to jointly refine both the point cloud model and the patch-wise trigger, ensuring optimal effectiveness and stealthiness of the trigger. Our main contributions include:

- We propose SPBA, which introduces the first patch-wise trigger for 3D point cloud backdoor attack based on the Graph Fourier Transform (GFT), enabling precise local spectral perturbations while preserving global geometric structure.
- We introduce a curvature-based patch imperceptibility scoring mechanism to identify and select geometrically complex patches for trigger injection, significantly enhancing stealthiness by avoiding perturbations in smooth areas.
- Extensive experiments on ModelNet40 and ShapeNetPart demonstrate the superior attack performance and stealthiness of the proposed SPBA.

2. Related Work

2.1. Backdoor Attacks in 2D Image

Backdoor attacks pose a significant security threat to deep neural networks (DNNs) by embedding hidden triggers during the training phase, enabling adversaries to manipulate model predictions during inference [17]. The effectiveness of a backdoor attack heavily depends on trigger design, which can be broadly categorized into global triggers and local patch-wise triggers. Prior works have explored global triggers through image generation [15], image warping [23], and frequency-domain injection [6], significantly increasing the difficulty of detection. Additionally, optimization-based approaches [4, 39] refine global triggers using carefully designed objective functions, aiming to balance stealthiness and attack effectiveness. As for local patch-wise triggers, BadNets [9] first demonstrated the feasibility of backdoor attacks in the 2D image domain with a fix patch at the corner. Since then, patch-wise triggers have become a fundamental paradigm in backdoor attacks due to their high attack success rates and stealthiness. Chen *et al.* [3] introduced a blending strategy, embedding triggers with partial transparency to make them less detectable. Yuan *et al.* [42] found that Vision Transformers (ViTs) are particularly vulnerable to patch-wise triggers, due to their global dependencies within patches. Some works further explored the adaptability of patch-wise trigger to various training paradigms, including self-supervised learning [27] and multimodal contrastive learning [1]. Gao *et al.* [8] further improved patch-wise attacks by designing a sparse and invisible trigger through bi-level optimization, minimizing visual detectability while preserving attack effectiveness. What's more, Li *et al.* [16] adopted patch-wise triggers as a harmless and stealthy way to protect the dataset copyright.

However, existing local patch-wise trigger designs pri-

marily focus on 2D images, and their direct adaptation to 3D point clouds presents unique challenges due to the unordered and irregular structure of point cloud data. This motivates our work, which aims to explore optimized local patch-wise triggers for 3D point cloud models.

2.2. Backdoor Attacks in 3D Point Cloud

Recent studies have explored backdoor attacks in 3D point cloud, proposing various trigger designs based on their unique properties [13, 32]. PointBA [13] introduced two attack strategies: PointBA-I, which injects an additional cluster of points as a trigger, and PointBA-O, which exploits a specific rotation angle as the backdoor trigger. Similar to PointBA-I, PCBA [37] embeds a spherical point cloud at an optimized location to manipulate model predictions. To further enhance stealthiness, IRBA [7] achieved sample-specific triggers by utilizing a nonlinear and local transformation. Additionally, iBA [2] generated poisoned samples using a folding-based autoencoder (AE), introducing a sample-wise trigger consists of geometric perturbations during reconstruction. Among spectral-based approaches [11, 12, 20], IBAPC [5] optimized a sample-wise spectral trigger to balance global shape preservation with localized point perturbations. However, the above attack methods all rely on sample-wise trigger injection to generate poisoned samples, which inevitably introduces noticeable global geometric deformations or noise.

In contrast, our approach is the first to propose a local patch-wise trigger for 3D point cloud backdoor attacks, ensuring that perturbations remain confined to selected geometrically complex regions rather than affecting the entire structure. We observe that similar techniques have been employed in recent adversarial attacks [19, 38]. However, our approach differs from these methods in two key aspects: (1) Region selection strategy: Prior adversarial attacks leverage spectral analysis to filter and select different regions for perturbation. In contrast, our method introduces a curvature-based patch imperceptibility score and selects points based on individual patch level. (2) Attack paradigm: As test-time attacks, these adversarial attacks require sample-specific perturbations, which are optimized uniquely for each input in the spatial domain using region-specific optimization. In contrast, our backdoor attack is a train-time attack, requiring a unified patch-wise trigger that can be consistently embedded into local patches across different samples. This need for a local and transferable trigger motivates our spectral-domain design, ensuring that perturbations remain structurally coherent while maintaining high attack effectiveness.

3. Method

3.1. Problem Statement

We define a training dataset with N samples as $D = \{(P_i, Y_i)\}_{i=1}^N$, where $P_i \in \mathbb{R}^{n \times 3}$ represents the three-dimensional coordinates of a point cloud instance and its corresponding label Y_i belongs to a predefined set of K classes, i.e., $Y_i \in \{1, \dots, K\}$. Building upon the previous explanation [6, 9], we divide the training dataset into two subsets: a benign subset D_b and a poisoned subset D_p . The poisoned subset consists of a portion ρ of the training dataset D , where selected samples are manipulated by the trigger injection function \mathcal{T} (as shown in Figure 2) and their labels are modified to a predefined target label Y_t . Given that the attacker has full control over the training process and access to the entire dataset, the backdoored model f_θ trained on this training dataset maintains high accuracy on benign samples while consistently misclassifying any poisoned sample $P'_i = \mathcal{T}(P_i)$ as the target class Y_t .

3.2. Patchification and Curvature-Aware Selection

Due to the unordered and irregular nature of point clouds, it is infeasible to directly segment patches for trigger injection in the same manner as in 2D images. To address this challenge, we draw inspiration from previous works [43, 46] and employ Farthest Point Sampling (FPS) and K-Nearest Neighbors (KNN) algorithms to systematically decompose each point cloud into local patches. This approach ensures a structured yet flexible partitioning that facilitates effective curvature-aware patch selection for spectral trigger embedding. Given an input point cloud sample P , FPS is first applied to select g center points $P^{ct} = \{p_1^{ct}, p_1^{ct}, \dots, p_g^{ct}\}$, ensuring a well-distributed set of key reference points. For each center point $p^{ct} \in P^{ct}$, a local patch will be constructed by the KNN algorithm containing k_p neighbors: $S_i = KNN(P, p^{ct})$ where $S_i \in \mathbb{R}^{k_p \times 3}$. Each local patch captures fine-grained geometric information, enabling the assessment of its structural complexity for curvature-aware selection. The resulting set of patches is represented as $\{S_1, S_2, \dots, S_g\}$.

As human visual sensitivity varies across different regions of a 3D object, perturbations in high-complexity patches are less perceptible due to the absence of a fixed prior shape. We define a patch imperceptibility score (PIS), which draws from the imperceptibility score concept of the saliency and imperceptibility score (SI score) [22]. However, our PIS is specifically designed to focus on patch-wise geometric complexity without incorporating the saliency score. The local curvature around each point p_j is defined as:

$$C(p_j) = \frac{1}{k_c} \sum_{q \in \mathcal{N}_{p_j}} \left| \left\langle \frac{q - p_j}{\|q - p_j\|_2}, \mathbf{n}_{p_j} \right\rangle \right|, \quad (1)$$

where \mathcal{N}_{p_j} represents the j -th patch with k_c nearest neigh-

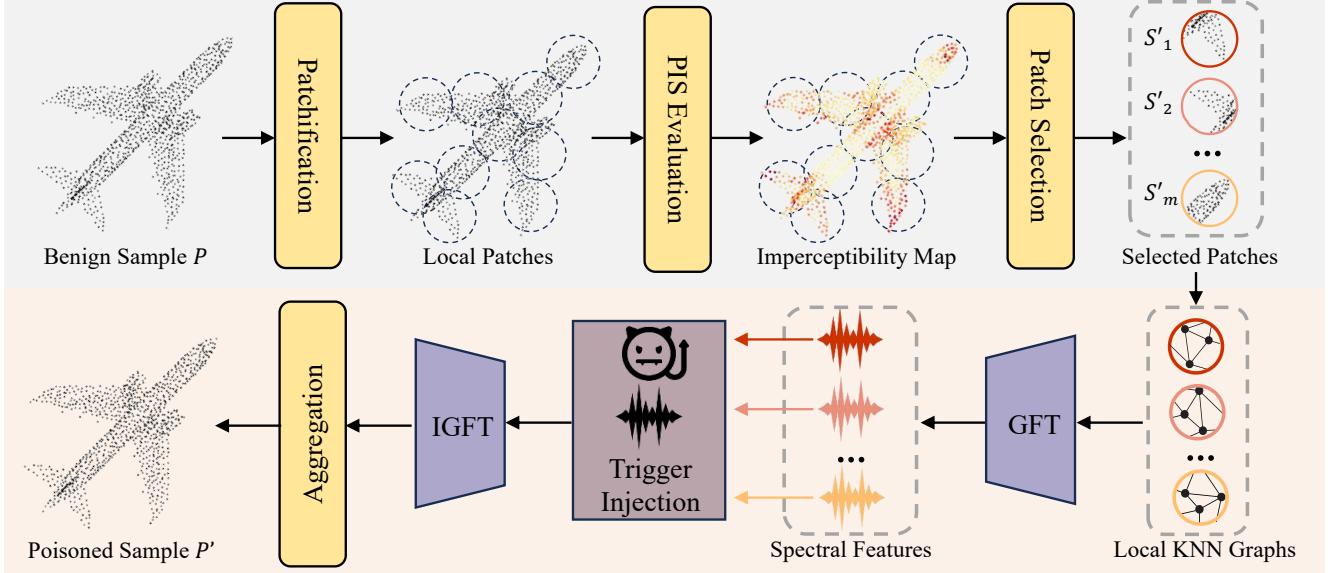


Figure 2. The framework of our proposed SPBA method. Given a benign point cloud sample P , SPBA first decomposes the sample into local patches and evaluates their patch imperceptibility scores (PIS). Patches with high PIS are then selected and transformed into the spectral domain using the Graph Fourier Transform (GFT). A spectral trigger is injected into the selected patches, ensuring stealthy perturbations. Finally, the Inverse Graph Fourier Transform (IGFT) reconstructs the local patches, which are then aggregated with the unmodified patches to form the final poisoned sample P' .

bor of point p_j and \mathbf{n}_{p_j} denotes its normal vector. To evaluate imperceptibility, the imperceptibility score (IS) of a certain point is computed as the standard deviation of curvature between the point p_j and its neighboring points N_{p_j} , capturing local curvature fluctuations:

$$IS(p_j) = \sqrt{\frac{1}{k_c} \sum_{q \in N_{p_j}} (C(q) - \frac{1}{k_c} \sum_{q \in N_{p_j}} C(q))^2}. \quad (2)$$

Using this measure, we construct an imperceptibility map for the entire point cloud. Finally, the patch imperceptibility score (PIS) of local patch S is calculated by averaging score of all points within the patch:

$$PIS(S) = \frac{1}{k_p} \sum_{p \in S} IS(p). \quad (3)$$

From the generated patches, we select the top m patches $\{S'_1, S'_2, \dots, S'_m\}$ with the highest PIS for subsequent trigger injection, ensuring that perturbations remain both effective and inconspicuous.

3.3. Patch-wise Spectral Trigger Injection

Designing local patch-wise triggers for 3D point clouds presents significant challenges due to their unordered and irregular structure, which limits the transferability of spatial local triggers across samples. When injected into different regions of different point cloud instances, these triggers often introduce noticeable outliers and cause severe semantic

distortions, ultimately compromising both stealthiness and attack effectiveness.

To overcome these limitations, we propose designing local patch-wise triggers in the spectral domain [12, 20]. Specially, a selected point cloud patch $S' \in \{S'_1, S'_2, \dots, S'_m\}$ is first transformed into an unweighted KNN graph $G = (V, A)$. Here $V \in \mathbb{R}^{k_p \times 3}$ represents the set of vertices, where each vertex corresponds to a point in the patch S' and connects to its k_g -nearest neighbors. The adjacency matrix $A \in \mathbb{R}^{k_p \times k_p}$ encodes connectivity among points, where $A_{ij} = 1$ if point i and j are connected otherwise $A_{ij} = 0$. From this, we compute the combinatorial graph Laplacian matrix [29] defined as $L = D - A$, where $D \in \mathbb{R}^{k_p \times k_p}$ is the degree matrix, with each entry defined as $D_{ij} = \sum_{j=1}^N A_{ij}$. Since L is real, symmetric, and positive semi-definite, we perform eigen decomposition on it as $L = U\Lambda U^T$, where $U \in \mathbb{R}^{k_p \times k_p}$ is an orthonormal matrix containing the eigenvectors and Λ consists of eigenvalues.

Using this decomposition, we compute the spectral feature of S' via the Graph Fourier Transform (GFT), where low-spectrum components capture coarse structural information, while high-spectrum components encode fine-grained geometric details:

$$\hat{S} = \phi_{GFT}(S') = U^T S', \quad (4)$$

where $\hat{S} \in \mathbb{R}^{k_p \times 3}$. Correspondingly, the Inverse GFT (IGFT) could reconstruct the spatial feature from the spec-

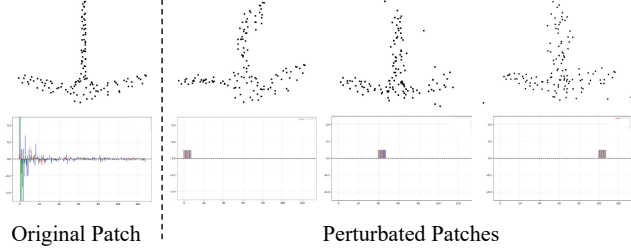


Figure 3. Comparison of original and perturbed patches. The second row shows the spectral features of the original patch and spectral perturbations across different spectrum bands.

tral domain:

$$S' = \phi_{IGFT}(\hat{S}) = U\hat{S}'. \quad (5)$$

As illustrated in Figure 3, low-spectrum perturbations cause significant deformation to the patch of empennage, while high-spectrum perturbations introduce excessive outliers. Perturbations applied within intermediate spectral bands mitigate outliers while preserving the overall shape, presenting a key challenge for optimal spectral trigger design. To address this, we propose an optimizable spectral trigger $\xi \in \mathbb{R}^{k_p \times 3}$, which is applied to the spectral features of selected patches to generate the poisoned patches S^p :

$$S^p = \phi_{IGFT}(\phi_{GFT}(S') + \xi), \quad (6)$$

where $S' \in \{S'_1, S'_2, \dots, S'_m\}$. The final poisoned point cloud sample P' is then constructed by replacing the original selected patches with the reconstructed patches while keeping the unselected regions unchanged:

$$P' = \mathcal{T}(P) = (P \setminus \{S'_1, S'_2, \dots, S'_m\}) \cup \{S^p_1, S^p_2, \dots, S^p_m\}. \quad (7)$$

3.4. Optimization Strategy

The backdoor learning process follows an alternating optimization scheme, where the model parameters θ and the spectral trigger ξ are updated iteratively, with one being optimized while the other remains frozen. Thus, each optimization step consists of two forward and backward propagations.

To train the model parameters θ , we define the loss function L_M , following the standard formulation for backdoor attacks:

$$L_M = \sum_{(P,Y) \in D_b} L_{CE}(f_\theta(P), Y) + \sum_{(P',Y_t) \in D_p} L_{CE}(f_\theta(P'), Y_t), \quad (8)$$

where L_{CE} represents the cross-entropy loss function.

To optimize the patch-wise trigger ξ for both attack efficiency and high stealthiness, we ensure that poisoned samples are misclassified into the target class Y_t while maintaining minimal perceptual distortions. This is achieved

through the following loss function L_T :

$$L_T = \sum_{(P,Y) \in D} (L_{CE}(f_\theta(\mathcal{T}(P)), Y_t) + L_{reg}(P, \mathcal{T}(P))). \quad (9)$$

In the regularizer function L_{reg} , we employ Euclidean distance (ED) and Chamfer distance (CD) [36] to enforce similarity between the original and poisoned point clouds, and Hausdorff distance (HD) [33] is used to control the worst scenario of outliers. The final regularization term is formulated as:

$$L_{reg} = \lambda_1 L_{ED}(P, \mathcal{T}(P)) + \lambda_2 L_{CD}(P, \mathcal{T}(P)) + \lambda_3 L_{HD}(P, \mathcal{T}(P)), \quad (10)$$

where $\lambda_1, \lambda_2, \lambda_3$ control the relative contribution of each loss term. This joint optimization framework ensures that the spectral trigger remains both effective and imperceptible, enabling stealthy backdoor attacks on 3D point cloud models.

4. Experiments and Results

4.1. Experiment Details

Datasets and Models. We evaluate our proposed method on two widely used 3D point cloud classification datasets: 1) ModelNet40 [34]: a benchmark dataset containing 40 object categories, with an official split of 9,843 training samples and 2,468 testing samples. 2) ShapeNetPart [40]: a subset of ShapeNet, consisting of 12,128 training samples and 2,874 testing samples across 16 object categories. For both datasets, we uniformly sample 1,024 points from each shape along with their normal vectors, normalizing the coordinates for consistency. For backdoored models, we adopted the most widely used models in previous work [7, 13], including PointNet [24], PointNet++ [25], DGCNN [31], and PointNext [26].

Attacks Setup. We compare our proposed SPBA method against four representative point cloud attack methods: PointBA-I [13], PointBA-O [13], IRBA [7], and IBAPC [5]. To reproduce PointBA-I, we implant a spherical cluster comprising 3% of the total points, with a fixed radius of 0.05, positioned at (0.5, 0.5, 0.5) in the coordinate space. For PointBA-O, we apply a 10° rotation along the Z-axis. For IRBA and IBAPC, we follow the default configurations specified in their original papers. For our proposed SPBA, g and k_p are both set as 32 for patch decomposition, while the values of k_c and k_g are both set as 10 for the KNN graph construction. And $m = 16$ patches are selected for trigger injection. For the regularizer function in Eq. 10, we set $\lambda_1 = 1$, $\lambda_2 = 5$ and $\lambda_3 = 1$. However, for PointNet, we adjust λ_1 to 0.1 to improve stability. For all attack methods, we set the poisoning rate $\rho = 0.1$. The target class is chosen as Chair ($Y_t = 8$) for ModelNet40 and Lamp ($Y_t = 8$)

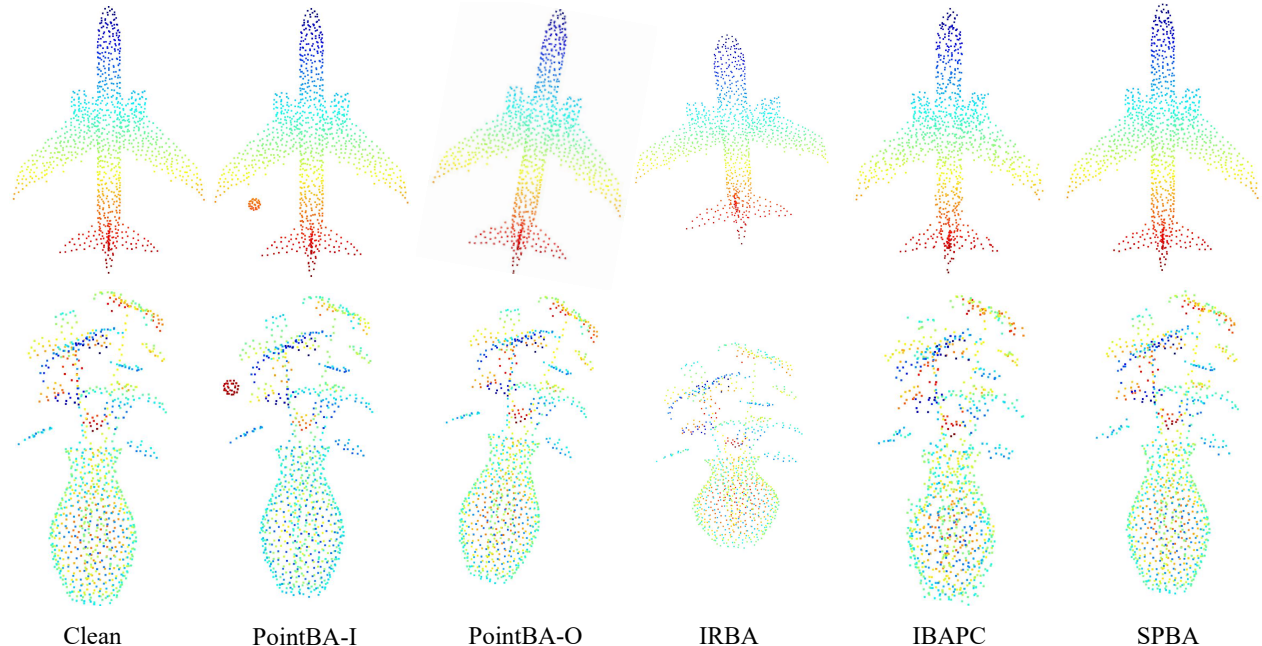


Figure 4. Visual comparison of poisoned samples from different backdoor attack methods. SPBA preserves structural integrity and ensures smooth regions (e.g., airplane body, vase) remain undisturbed, enhancing imperceptibility.

for ShapeNetPart. Two Adam optimizers are employed for backdoored models training and spectral trigger optimization, with learning rates of 0.001 and 0.01, respectively.

Evaluation Metrics. The attack performance can be evaluated by Benign Accuracy (BA) and Attack Success Rate (ASR). BA is the accuracy of benign test samples that are correctly classified. ASR represents the proportion of poisoned samples that are successfully misclassified into the target label. To quantify the imperceptibility of poisoned samples, we compute the Chamfer Distance (CD) between the poisoned and original samples. A successful backdoor attack should achieve a high ASR and lower CD while preserving BA as much as possible. For clarity, both BA and ASR are presented as percentages, and CD values in tables are scaled by a factor of 1,000.

4.2. Attack Effectiveness

As shown in Table 1, our proposed SPBA achieves an average BA of 89.02%, which is comparable to the clean model and exceeds most attack methods, ensuring that the model retains its normal classification performance. Although PointBA-I achieves the highest average ASR of 98.43%, it comes at the cost of a significantly higher average CD of 4.08, making it much more detectable. In contrast, SPBA maintains the lowest average CD of 1.08, highlighting its superior imperceptibility. What’s more, SPBA achieves an average ASR of 97.58%, surpassing transform-based attacks PointBA-O and IRBA by 1.89% and 3.49% respectively. Compared to the global spectral attack IBAPC,

SPBA not only achieves higher BA and ASR on average but also further reduces average CD by 0.34, demonstrating the stealthiness of injecting an optimized spectral trigger into geometrically complex patches. Table 2 shows more experiment results on ShapeNetpart. SPBA achieves the second-highest average ASR and BA while maintaining the lowest average CD, achieving the best balance between attack effectiveness and stealthiness. These results further establish SPBA as a more effective and imperceptible backdoor attack method compared to existing approaches.

4.3. Attack Stealthiness

We visualize some poisoned samples generated by different backdoor attack methods in Figure 4. As observed, PointBA-I introduces noticeable anomalies compared to clean samples, significantly increasing its detectability. Although PointBA-O and IRBA generate natural-looking poisoned samples by applying transformation, they still cause considerable deformations in shape. Compared to IBAPC, our proposed SPBA maintains the smoothness of regions with simple structures, thereby enhancing the imperceptibility of poisoned samples. For instance, in the flower pot example, SPBA selectively perturbs the flower region while preserving the smooth structure of the vase, making the modifications less perceptible to human observers.

4.4. Comparison of Spectral Triggers

Both SPBA and IBAPC involve spectral trigger design, but differ in their scope. SPBA applies a patch-wise spectral

Table 1. Comparison of attack performance across different models on ModelNet40. Both BA and ASR are presented as percentages, and CD values in tables are scaled by a factor of 1,000. The best results are **bolded** and the second-best results are underlined.

Model	Clean	PointBA-I			PointBA-O			IRBA			IBAPC			SPBA		
	BA↑	BA↑	ASR↑	CD↓	BA↑	ASR↑	CD↓	BA↑	ASR↑	CD↓	BA↑	ASR↑	CD↓	BA↑	ASR↑	CD↓
PointNet	89.14	89.67	99.03	4.08	88.17	94.77	5.31	88.25	93.27	18.54	88.42	94.15	<u>3.58</u>	<u>88.90</u>	<u>97.89</u>	2.60
PointNet++	90.80	<u>90.36</u>	98.87	4.08	89.55	96.68	5.31	90.40	<u>98.26</u>	18.54	90.72	96.11	<u>0.47</u>	89.42	97.97	0.11
DGCNN	89.75	91.05	100.00	4.08	89.67	95.02	5.31	89.55	92.38	18.54	88.04	97.44	0.54	<u>89.75</u>	<u>97.61</u>	<u>0.69</u>
PointNext	89.22	88.21	95.83	4.08	88.94	96.31	5.31	88.41	92.46	18.54	<u>88.70</u>	97.69	<u>1.09</u>	88.62	<u>96.85</u>	0.92
Average	89.73	89.82	98.43	4.08	89.08	95.69	5.31	89.15	94.09	18.54	88.97	96.35	<u>1.42</u>	<u>89.17</u>	<u>97.58</u>	1.08

Table 2. Comparison of attack performance across different models on ShapeNetPart. Both BA and ASR are presented as percentages, and CD values in tables are scaled by a factor of 1,000. The best results are **bolded** and the second-best results are underlined.

Model	Clean	PointBA-I			PointBA-O			IRBA			IBAPC			SPBA		
	BA↑	BA↑	ASR↑	CD↓	BA↑	ASR↑	CD↓	BA↑	ASR↑	CD↓	BA↑	ASR↑	CD↓	BA↑	ASR↑	CD↓
PointNet	98.47	98.30	99.72	7.48	97.95	98.34	5.67	<u>98.12</u>	96.80	16.06	97.98	95.86	<u>1.82</u>	98.30	<u>98.40</u>	1.22
PointNet++	98.99	98.75	99.69	7.48	<u>98.50</u>	98.78	5.67	98.89	<u>99.03</u>	16.06	98.47	98.92	<u>0.08</u>	98.26	98.30	0.02
DGCNN	99.06	98.92	100.00	7.48	<u>98.85</u>	98.50	5.67	98.68	97.63	16.06	97.36	98.68	<u>0.75</u>	98.43	<u>99.23</u>	0.44
PointNext	98.82	98.61	99.51	7.48	98.10	96.83	5.67	96.31	96.17	16.06	97.32	98.37	<u>0.67</u>	<u>98.53</u>	<u>98.45</u>	0.37
Average	98.83	98.64	99.73	7.48	98.35	98.11	5.67	98.00	97.41	16.06	97.78	97.96	<u>0.83</u>	<u>98.38</u>	<u>98.60</u>	0.51

trigger independently to the 16 patches with the highest PSI, whereas IBAPC employs a global spectral trigger that affects the entire sample. To analyze the impact of perturbation localization, we evaluate the well-trained spectral trigger on the ModelNet40 test dataset using PointNet++, which only affects the ASR and CD of backdoored models on the poisoned data. Specially, we decompose the trigger of IBAPC into IBAPC-H16 (confined to complex regions) and IBAPC-L (confined to smooth regions). As shown in Table 4, IBAPC-L achieves a 20.29% higher average ASR than IBAPC-H16 under near-intensity perturbations. This result suggests that IBAPC relies more on smooth-region perturbations, which reduce imperceptibility, as illustrated in Figure 4. For a fair comparison, we introduce SPBA-H8, a weaker test version of our method, which applies the patch-wise trigger to only eight complex patches during inference, further minimizing perturbation intensity. However, SPBA-H8 still surpasses IBAPC-L and IBAPC-H16 in ASR by 14.79% and 35.08%, respectively, while maintaining the lowest CD. This highlights the effectiveness of patch-wise spectral triggers in achieving an optimal balance between attack performance and stealthiness.

4.5. Resistance to Defense Methods

Resistance to Data Augmentation. Since data augmentation is widely employed to enhance the robustness of classification models, we introduce six types of augmentations to evaluate their impact on backdoor attack performance: 1)

Rotation: random rotation around the z-axis with a maximum angle of 10° ; 2) Rotation3D: random rotation up to 10° along all three axes; 3) Scaling: scaling within a range of 0.5 to 1.5; 4) Shift: shifting randomly between -0.1 and 0.1 along each axis; 5) Dropout: removing up to 20% of points; and 6) Jitter: introducing noise sampled from $N(0, 0.02)$. The experiments are conducted on the ModelNet40 dataset using the PointNet++ model. As shown in Table 3, different augmentations affect attack methods to varying degrees. Due to the high visibility of the trigger of PointBA-I, augmentations have minimal impact, as the trigger remains distinct. However, for rotation-based PointBA-O, applying Rotation significantly reduces attack effectiveness. For IRBA, which relies on local transformations, augmentations such as Rotation3D, Dropout and Jitter cause a notable decline in attack performance, with ASR dropping by up to 8.23%. Conversely, for optimization-based attacks like IBAPC and our proposed SPBA, only Jitter leads to a slight ASR reduction, while other augmentations have negligible effects, demonstrating their robustness against most augmentations.

Resistance to SOR. Statistical Outlier Removal (SOR) [45] is a widely used technique designed to eliminate outliers based on the local neighborhood density, determined by the KNN algorithm. In our implementation, we set KNN to use 40 nearest neighbors and set the standard deviation threshold to 1. To assess the impact of SOR on backdoor attack performance, we apply it during inference on Point-

Table 3. Resistance of backdoor attacks against varied data augmentations

Augmentation	PointBA-I		PointBA-O		IRBA		IBAPC		SPBA	
	BA \uparrow	ASR \uparrow								
No	90.36	98.87	89.55	96.68	90.40	98.26	90.72	96.11	89.42	97.97
Rotation	89.42	98.95	86.83	7.66	90.52	97.69	89.91	95.95	89.34	98.22
Rotation3D	89.71	99.11	88.78	30.51	90.68	92.79	90.24	95.34	89.38	97.24
Scaling	90.72	99.55	91.65	96.92	91.17	99.47	91.49	97.08	91.57	98.26
Shift	90.11	99.03	89.67	96.07	90.03	97.93	90.52	95.99	89.59	97.08
Dropout	90.52	99.39	90.07	96.11	90.40	94.85	91.05	95.02	90.76	97.24
Jitter	89.42	98.70	89.34	95.06	90.07	90.03	90.64	92.18	90.96	95.01

Table 4. Comparison of attack performance between IBAPC and SPBA with varied poisoned patches.

Method	IBAPC-L		IBAPC-H16		SPBA-H8	
	ASR \uparrow	CD \downarrow	ASR \uparrow	CD \downarrow	ASR \uparrow	CD \downarrow
PointNet	61.75	1.93	46.03	1.65	86.10	1.39
PointNet++	85.66	0.25	66.53	0.22	85.90	0.06
DGCNN	69.00	0.26	46.88	0.28	83.91	0.32
PointNext	57.82	0.61	33.63	0.48	77.47	0.35
Average	68.56	0.76	48.27	0.66	83.35	0.53

Table 5. Comparison of attack performance of SPBA with various patch selection strategies.

Strategy	H-PSI	L-PSI	HD	LD	Random
BA \uparrow	89.42	88.82	89.23	89.14	89.30
ASR \uparrow	97.97	95.58	97.45	96.07	97.20
CD \downarrow	0.11	0.14	0.12	0.11	0.13

Net++ models trained on ModelNet40. Results show that only PointBA-I experiences a significant ASR reduction of 22.94%, as SOR effectively removes its trigger points as outliers. This suggests that SOR serves as an effective defense specifically against injection-based attacks while having limited impact on other attack methods.

Resistance to the Gradient-based Method. As many studies on backdoor attacks assess trigger stealthiness using gradient-based methods [23, 28], we employ a point cloud saliency map [44] to identify salient points that contribute most to the model’s decision-making. Specially, 40 points with the highest saliency scores are marked in red. As illustrated in Figure 5, the spherical trigger of PointBA-I is easily detected. In contrast, our proposed SPBA exhibits a saliency distribution similar to the clean model, indicating enhanced stealthiness and reduced detectability.

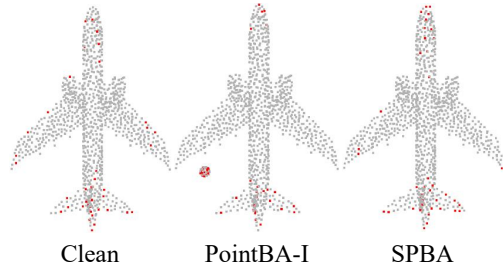


Figure 5. Gradient-based saliency analysis with the most significant points highlighted in red.

4.6. Ablation Study

Effect of Patch Selection Strategies. In our default setting, we select the 16 patches with the highest patch imperceptibility scores (PIS), denoted as H-PSI. To evaluate the effectiveness of this selection strategy, we compare H-PSI with four alternative patch selection strategies: (1) L-PSI: Select the patches with the lowest PIS. (2) HD: Select the patches with the highest patch densities, computed as the sum of distances from points to their respective patch central points. (3) LD: Select the patches with the lowest patch densities. (4) Random: Randomly select the patches. We evaluate their impact on ModelNet40 using the PointNet++ model. As shown in Table 5, the H-PSI strategy achieves the highest attack effectiveness and the strongest stealthiness. This result underscores the advantage of selecting high-imperceptibility patches for local spectral trigger injection.

5. Conclusion

In this paper, we propose SPBA, a novel backdoor attack method against 3D point cloud models. Unlike existing methods that rely on sample-wise trigger injection, which introduces noticeable geometric distortions, SPBA employs a local patch-wise trigger that selectively perturbs geometrically complex regions. By leveraging Graph Fourier Transform, our proposed patch-wise trigger minimizes geomet-

ric deformations while maintaining high attack effectiveness. Experimental results on ModelNet40 and ShapeNet-Part demonstrate that SPBA achieves a high attack success rate with minimal perceptibility, outperforming prior sample-wise backdoor attacks in stealthiness. These findings highlight the effectiveness of patch-wise triggers as a promising direction for stealthy and adaptive backdoor attacks in 3D deep learning.

References

- [1] Jiawang Bai, Kuofeng Gao, Shaobo Min, Shu-Tao Xia, Zhifeng Li, and Wei Liu. Badclip: Trigger-aware prompt learning for backdoor attacks on clip. In *Proceedings of the IEEE/CVF Conference on Computer Vision and Pattern Recognition (CVPR)*, pages 24239–24250, 2024. 2
- [2] Yuhao Bian, Shengjing Tian, and Xiuping Liu. iba: Backdoor attack on 3d point cloud via reconstructing itself. *IEEE Transactions on Information Forensics and Security (TIFS)*, 2024. 3
- [3] Xinyun Chen, Chang Liu, Bo Li, Kimberly Lu, and Dawn Song. Targeted backdoor attacks on deep learning systems using data poisoning. *arXiv preprint arXiv:1712.05526*, 2017. 2
- [4] Khoa Doan, Yingjie Lao, Weijie Zhao, and Ping Li. Lira: Learnable, imperceptible and robust backdoor attacks. In *Proceedings of the IEEE/CVF Conference on Computer Vision and Pattern Recognition (CVPR)*, pages 11966–11976, 2021. 2
- [5] Linkun Fan, Fazhi He, Tongzhen Si, Wei Tang, and Bing Li. Invisible backdoor attack against 3d point cloud classifier in graph spectral domain. In *Proceedings of the AAAI Conference on Artificial Intelligence (AAAI)*, pages 21072–21080, 2024. 1, 2, 3, 5
- [6] Yu Feng, Benteng Ma, Jing Zhang, Shanshan Zhao, Yong Xia, and Dacheng Tao. Fiba: Frequency-injection based backdoor attack in medical image analysis. In *Proceedings of the IEEE/CVF Conference on Computer Vision and Pattern Recognition (CVPR)*, pages 20876–20885, 2022. 2, 3
- [7] Kuofeng Gao, Jiawang Bai, Baoyuan Wu, Mengxi Ya, and Shu-Tao Xia. Imperceptible and robust backdoor attack in 3d point cloud. *IEEE Transactions on Information Forensics and Security (TIFS)*, 19:1267–1282, 2023. 1, 2, 3, 5
- [8] Yinghua Gao, Yiming Li, Xueluan Gong, Zhifeng Li, Shu-Tao Xia, and Qian Wang. Backdoor attack with sparse and invisible trigger. *IEEE Transactions on Information Forensics and Security (TIFS)*, 2024. 2
- [9] Tianyu Gu, Kang Liu, Brendan Dolan-Gavitt, and Siddharth Garg. Badnets: Evaluating backdooring attacks on deep neural networks. *IEEE Access*, 7:47230–47244, 2019. 2, 3
- [10] Yulan Guo, Hanyun Wang, Qingyong Hu, Hao Liu, Li Liu, and Mohammed Bennis. Deep learning for 3d point clouds: A survey. *IEEE Transactions on Pattern Analysis and Machine Intelligence (PAMI)*, 43(12):4338–4364, 2020. 1
- [11] Yuehui Han, Jiaxin Chen, Jianjun Qian, and Jin Xie. Graph spectral perturbation for 3d point cloud contrastive learning. In *Proceedings of the 31st ACM International Conference on Multimedia (MM)*, pages 5389–5398, 2023. 3
- [12] Qianjiang Hu, Daizong Liu, and Wei Hu. Exploring the devil in graph spectral domain for 3d point cloud attacks. In *European Conference on Computer Vision (ECCV)*, pages 229–248. Springer, 2022. 3, 4
- [13] Xinke Li, Zhirui Chen, Yue Zhao, Zekun Tong, Yabang Zhao, Andrew Lim, and Joey Tianyi Zhou. Pointba: Towards backdoor attacks in 3d point cloud. In *Proceedings of the IEEE/CVF International Conference on Computer Vision (ICCV)*, pages 16492–16501, 2021. 1, 3, 5
- [14] Ying Li, Lingfei Ma, Zilong Zhong, Fei Liu, Michael A Chapman, Dongpu Cao, and Jonathan Li. Deep learning for lidar point clouds in autonomous driving: A review. *IEEE Transactions on Neural Networks and Learning Systems (TNNLS)*, 32(8):3412–3432, 2020. 1
- [15] Yuezun Li, Yiming Li, Baoyuan Wu, Longkang Li, Ran He, and Siwei Lyu. Invisible backdoor attack with sample-specific triggers. In *Proceedings of the IEEE/CVF International Conference on Computer Vision (ICCV)*, pages 16463–16472, 2021. 2
- [16] Yiming Li, Yang Bai, Yong Jiang, Yong Yang, Shu-Tao Xia, and Bo Li. Untargeted backdoor watermark: Towards harmless and stealthy dataset copyright protection. *Advances in Neural Information Processing Systems (NeurIPS)*, 35:13238–13250, 2022. 2
- [17] Yiming Li, Yong Jiang, Zhifeng Li, and Shu-Tao Xia. Backdoor learning: A survey. *IEEE Transactions on Neural Networks and Learning Systems (TNNLS)*, 35(1):5–22, 2022. 2
- [18] Siyuan Liang, Mingli Zhu, Aishan Liu, Baoyuan Wu, Xiaochun Cao, and Ee-Chien Chang. Badclip: Dual-embedding guided backdoor attack on multimodal contrastive learning. In *Proceedings of the IEEE/CVF Conference on Computer Vision and Pattern Recognition (CVPR)*, pages 24645–24654, 2024. 1
- [19] Daizong Liu and Wei Hu. Explicitly perceiving and preserving the local geometric structures for 3d point cloud attack. In *Proceedings of the AAAI Conference on Artificial Intelligence (AAAI)*, pages 3576–3584, 2024. 3
- [20] Daizong Liu, Wei Hu, and Xin Li. Point cloud attacks in graph spectral domain: When 3d geometry meets graph signal processing. *IEEE Transactions on Pattern Analysis and Machine Intelligence (PAMI)*, 46(5):3079–3095, 2023. 3, 4
- [21] Yifan Liu, Wuyang Li, Jie Liu, Hui Chen, and Yixuan Yuan. Grab-net: Graph-based boundary-aware network for medical point cloud segmentation. *IEEE Transactions on Medical Imaging (TMI)*, 42(9):2776–2786, 2023. 1
- [22] Tianrui Lou, Xiaojun Jia, Jindong Gu, Li Liu, Siyuan Liang, Bangyan He, and Xiaochun Cao. Hide in thicket: Generating imperceptible and rational adversarial perturbations on 3d point clouds. In *Proceedings of the IEEE/CVF Conference on Computer Vision and Pattern Recognition (CVPR)*, pages 24326–24335, 2024. 2, 3
- [23] Tuan Anh Nguyen and Anh Tuan Tran. Wanet - imperceptible warping-based backdoor attack. In *International Conference on Learning Representations (ICLR)*, 2021. 2, 8
- [24] Charles R Qi, Hao Su, Kaichun Mo, and Leonidas J Guibas. Pointnet: Deep learning on point sets for 3d classification

- and segmentation. In *Proceedings of the IEEE/CVF Conference on Computer Vision and Pattern Recognition (CVPR)*, pages 652–660, 2017. 5
- [25] Charles Ruizhongtai Qi, Li Yi, Hao Su, and Leonidas J Guibas. Pointnet++: Deep hierarchical feature learning on point sets in a metric space. *Advances in Neural Information Processing Systems (NeurIPS)*, 30, 2017. 5
- [26] Guocheng Qian, Yuchen Li, Houwen Peng, Jinjie Mai, Hasan Hammoud, Mohamed Elhoseiny, and Bernard Ghanem. Pointnext: Revisiting pointnet++ with improved training and scaling strategies. *Advances in Neural Information Processing Systems (NeurIPS)*, 35:23192–23204, 2022. 5
- [27] Aniruddha Saha, Ajinkya Tejankar, Soroush Abbasi Koohpayegani, and Hamed Pirsiavash. Backdoor attacks on self-supervised learning. In *Proceedings of the IEEE/CVF Conference on Computer Vision and Pattern Recognition (CVPR)*, pages 13337–13346, 2022. 2
- [28] Ramprasaath R Selvaraju, Michael Cogswell, Abhishek Das, Ramakrishna Vedantam, Devi Parikh, and Dhruv Batra. Grad-cam: Visual explanations from deep networks via gradient-based localization. In *Proceedings of the IEEE/CVF International Conference on Computer Vision (ICCV)*, pages 618–626, 2017. 8
- [29] David I Shuman, Sunil K Narang, Pascal Frossard, Antonio Ortega, and Pierre Vandergheynst. The emerging field of signal processing on graphs: Extending high-dimensional data analysis to networks and other irregular domains. *IEEE Signal Processing Magazine (SPM)*, 30(3):83–98, 2013. 4
- [30] Hossein Souri, Liam Fowl, Rama Chellappa, Micah Goldblum, and Tom Goldstein. Sleeper agent: Scalable hidden trigger backdoors for neural networks trained from scratch. *Advances in Neural Information Processing Systems (NeurIPS)*, 35:19165–19178, 2022. 1
- [31] Yue Wang, Yongbin Sun, Ziwei Liu, Sanjay E Sarma, Michael M Bronstein, and Justin M Solomon. Dynamic graph cnn for learning on point clouds. *ACM Transactions on Graphics (TOG)*, 38(5):1–12, 2019. 5
- [32] Cheng Wei, Yang Wang, Kuofeng Gao, Shuo Shao, Yiming Li, Zhibo Wang, and Zhan Qin. Pointncbw: Towards dataset ownership verification for point clouds via negative clean-label backdoor watermark. *IEEE Transactions on Information Forensics and Security (TIFS)*, 2024. 3
- [33] Yuxin Wen, Jiehong Lin, Ke Chen, CL Philip Chen, and Kui Jia. Geometry-aware generation of adversarial point clouds. *IEEE Transactions on Pattern Analysis and Machine Intelligence (PAMI)*, 44(6):2984–2999, 2020. 5
- [34] Zhirong Wu, Shuran Song, Aditya Khosla, Fisher Yu, Linguang Zhang, Xiaoou Tang, and Jianxiong Xiao. 3d shapenets: A deep representation for volumetric shapes. In *Proceedings of the IEEE/CVF Conference on Computer Vision and Pattern Recognition (CVPR)*, pages 1912–1920, 2015. 5
- [35] Jun Xia, Zhihao Yue, Yingbo Zhou, Zhiwei Ling, Yiyu Shi, Xian Wei, and Mingsong Chen. Waveattack: Asymmetric frequency obfuscation-based backdoor attacks against deep neural networks. *Advances in Neural Information Processing Systems (NeurIPS)*, 37:43549–43570, 2025. 1
- [36] Chong Xiang, Charles R. Qi, and Bo Li. Generating 3d adversarial point clouds. In *Proceedings of the IEEE/CVF Conference on Computer Vision and Pattern Recognition (CVPR)*, 2019. 5
- [37] Zhen Xiang, David J Miller, Siheng Chen, Xi Li, and George Kesidis. A backdoor attack against 3d point cloud classifiers. In *Proceedings of the IEEE/CVF International Conference on Computer Vision (ICCV)*, pages 7597–7607, 2021. 1, 3
- [38] Mingyu Yang, Daizong Liu, Keke Tang, Pan Zhou, Lixing Chen, and Junyang Chen. Hiding imperceptible noise in curvature-aware patches for 3d point cloud attack. In *European Conference on Computer Vision (ECCV)*, pages 431–448. Springer, 2024. 3
- [39] Sheng Yang, Jiawang Bai, Kuofeng Gao, Yong Yang, Yiming Li, and Shu-Tao Xia. Not all prompts are secure: A switchable backdoor attack against pre-trained vision transformers. In *Proceedings of the IEEE/CVF Conference on Computer Vision and Pattern Recognition (CVPR)*, pages 24431–24441, 2024. 2
- [40] Li Yi, Vladimir G Kim, Duygu Ceylan, I-Chao Shen, Mengyan Yan, Hao Su, Cewu Lu, Qixing Huang, Alla Sheffer, and Leonidas Guibas. A scalable active framework for region annotation in 3d shape collections. *ACM Transactions on Graphics (TOG)*, 35(6):1–12, 2016. 5
- [41] Jianhui Yu, Chaoyi Zhang, Heng Wang, Dingxin Zhang, Yang Song, Tiange Xiang, Dongnan Liu, and Weidong Cai. 3d medical point transformer: Introducing convolution to attention networks for medical point cloud analysis. *arXiv preprint arXiv:2112.04863*, 2021. 1
- [42] Zenghui Yuan, Pan Zhou, Kai Zou, and Yu Cheng. You are catching my attention: Are vision transformers bad learners under backdoor attacks? In *Proceedings of the IEEE/CVF Conference on Computer Vision and Pattern Recognition (CVPR)*, pages 24605–24615, 2023. 1, 2
- [43] Renrui Zhang, Ziyu Guo, Peng Gao, Rongyao Fang, Bin Zhao, Dong Wang, Yu Qiao, and Hongsheng Li. Point-m2ae: multi-scale masked autoencoders for hierarchical point cloud pre-training. *Advances in Neural Information Processing Systems (NeurIPS)*, 35:27061–27074, 2022. 3
- [44] Tianhang Zheng, Changyou Chen, Junsong Yuan, Bo Li, and Kui Ren. Pointcloud saliency maps. In *Proceedings of the IEEE/CVF International Conference on Computer Vision (ICCV)*, pages 1598–1606, 2019. 8
- [45] Hang Zhou, Kejiang Chen, Weiming Zhang, Han Fang, Wenbo Zhou, and Nenghai Yu. Dup-net: Denoiser and up-sampler network for 3d adversarial point clouds defense. In *Proceedings of the IEEE/CVF International Conference on Computer Vision (ICCV)*, pages 1961–1970, 2019. 1, 7
- [46] Xin Zhou, Dingkan Liang, Wei Xu, Xingkui Zhu, Yihan Xu, Zhikang Zou, and Xiang Bai. Dynamic adapter meets prompt tuning: Parameter-efficient transfer learning for point cloud analysis. In *Proceedings of the IEEE/CVF Conference on Computer Vision and Pattern Recognition (CVPR)*, pages 14707–14717, 2024. 3
- [47] Haoyi Zhu, Yating Wang, Di Huang, Weicai Ye, Wanli Ouyang, and Tong He. Point cloud matters: Rethinking the impact of different observation spaces on robot learning. *Ad-*

Appendix

A. Ablation Study

A.1. Effect of the Target Class Y_t

In this section, we investigate the effect of different target classes on our attack performance. Specifically, we select the top 8 categories from ModelNet40 as target classes and conduct experiments using PointNet++. As shown in Figure 6, the choice of target class has a minimal effect on both Attack Success Rate (ASR) and Benign Accuracy (BA), with fluctuations not exceeding 1%. These results demonstrate the robustness of our approach across various target label settings, ensuring its consistency in different attack scenarios.

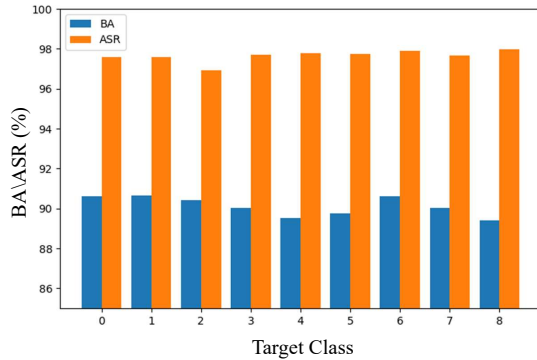


Figure 6. Effect of the target class selection.

A.2. Effect of the Poisoning Rate ρ

We explore the impact of the poisoning rate on our attack by conducting experiments on ModelNet40 using PointNet++. As shown in Figure 7, ASR consistently increases as the poisoning ratio rises, peaking at 98.42%. BA exhibits minor fluctuations but remains relatively stable as the poisoning rate increases. Notably, even at a low poisoning rate of 2.5%, our approach achieves an ASR of 96.27%, underscoring its effectiveness even with limited poisoned data.

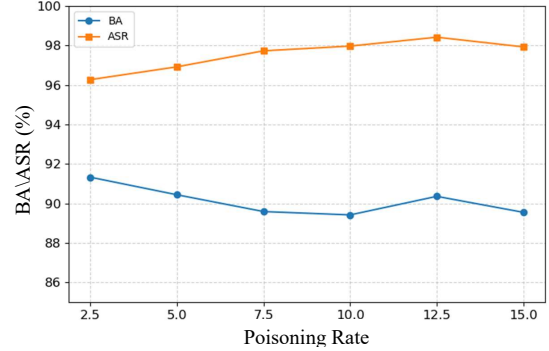


Figure 7. The effect of the poisoning rate.

A.3. Effect of the Selected Patch Number m

In this section, we experiment with injecting the spectral trigger into varying numbers m of selected patches during the training process. The experiments are conducted on ModelNet40 using PointNet++. As shown in Table 6, as m increases from 1 to 16, the Chamfer Distance (CD) gradually decreases, indicating improved stealthiness. This suggests that selecting more patches within a reasonable range helps distribute perturbations more naturally, enhancing imperceptibility. However, when m further increases to 32, where almost all points are perturbed, CD rises to 0.12, indicating that excessive modifications start to introduce noticeable distortions, reducing stealthiness. Based on these observations, we set $m = 16$ as the default configuration, as it achieves the optimal balance between imperceptibility (lowest CD), strong attack effectiveness, and stable benign accuracy.

B. Visualization on More Poisoned Samples

In Figure 8, we provide additional visualization results that highlight the exceptional stealthiness of our attack method. Our approach not only maintains the overall structural integrity of the poisoned samples but also ensures that smooth regions, such as the bottle body, chair legs, and car body, remain undisturbed. This careful preservation further enhances the imperceptibility of the attack.

Table 6. Effect of selected patch number m

m	1	2	4	8	16	24	32
BA	89.56	89.88	88.53	90.15	89.42	89.27	89.36
ASR	97.38	97.10	97.28	96.84	97.97	97.73	97.30
CD	0.17	0.19	0.18	0.14	0.11	0.11	0.12

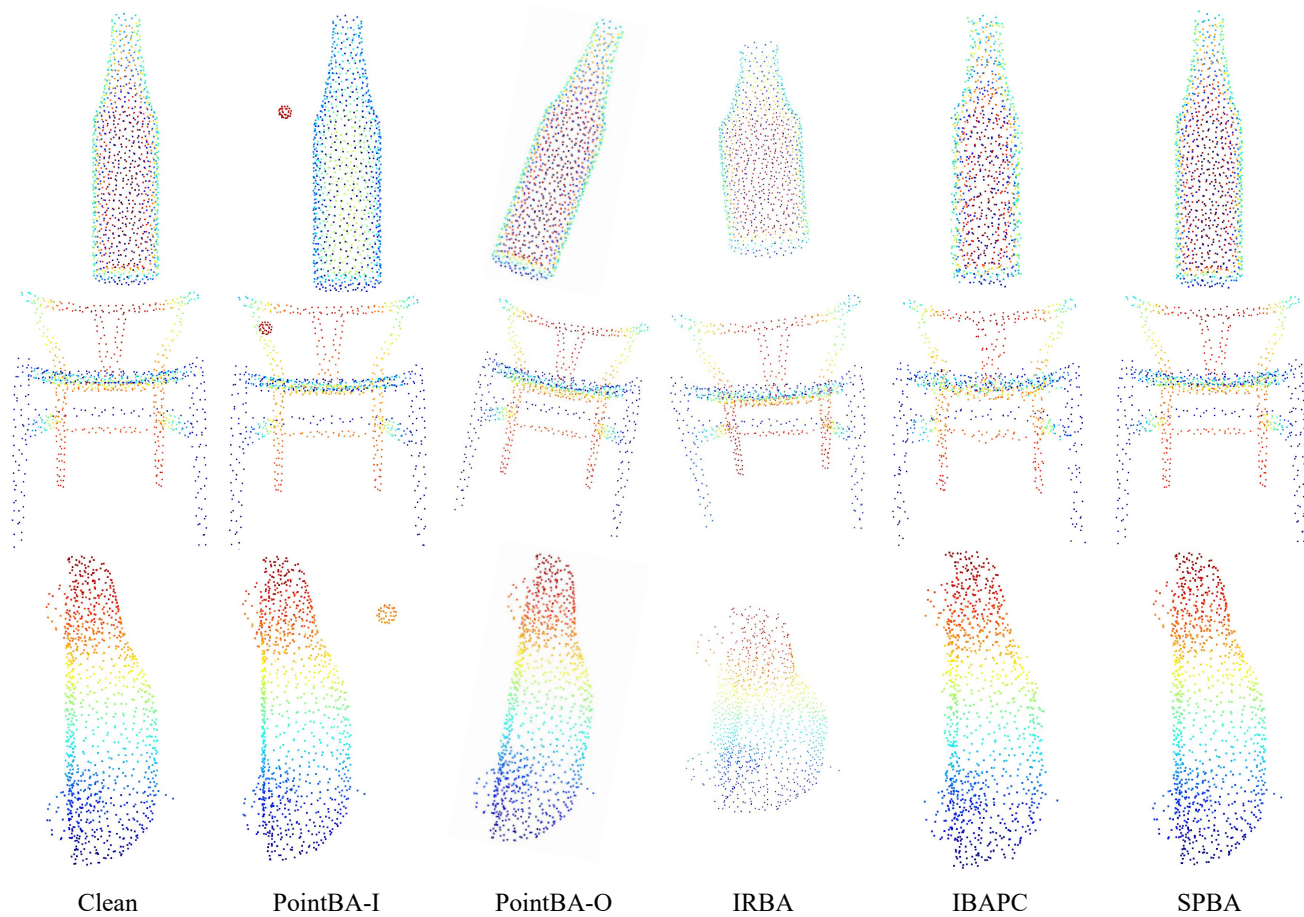


Figure 8. Visualization on more poisoned samples.